Physica E 61 (2014) 158–166

Contents lists available at ScienceDirect

Physica E

journal homepage: www.elsevier.com/locate/physe

Influence of the Al concentration on the electronic properties of coupled and uncoupled $Al_xGa_{1-x}As/AlAs/Al_yGa_{1-y}As$ double quantum wells

L.E.G. Armas [a,*], E.C.F. da Silva [b], C.A. Duarte [c,**], I.R. Pagnossin [b], A.A. Quivy [b], J.W. Menezes [a], C. Jacinto [d], A.C. Seabra [e], G.M. Gusev [b]

[a] Grupo de Óptica, Micro e Nanofabricação de Dispositivos – GOMNDI, Universidade Federal do Pampa – UNIPAMPA, Brazil
[b] Instituto de Física da Universidade de São Paulo, Laboratório de Novos Materiais Semicondutores (LNMS), CP 66318, 05315-970 São Paulo, SP, Brazil
[c] Departamento de Física, Centro Politécnico, Universidade Federal do Paraná, CP 81531-990 Curitiba, Paraná, Brazil
[d] Grupo de Fotônica e Fluidos Complexos, Instituto de Física, Universidade Federal de Alagoas – UFAL, Maceio, Alagoas 57072-970, Brazil
[e] Laboratório de Sistemas Integráveis do Departamento de Engenharia de Sistemas Eletrônicos da Escola Politécnica da USP (LSI-PSI/EPUSP), CEP 05508-010 São Paulo, SP, Brazil

HIGHLIGHTS

- Effect of different Al concentration on the electronic properties of coupled and uncoupled double quantum wells.
- Shubnikov-de Haas, Hall measurements and fast Fourier transform method were used.
- Electronic properties decrease, increasing Al content within the quantum wells.
- Alloy scattering effect explains decreasing of the electronic properties.

ARTICLE INFO

Article history:
Received 31 January 2014
Received in revised form
31 March 2014
Accepted 2 April 2014
Available online 13 April 2014

Keywords:
Double quantum well
AlGaAs
Shubnikov-de Haas
Electronic property
2DEG

ABSTRACT

Shubnikov-de Haas (SdH) and Hall measurements have been used to investigate the electron densities and mobilities in a pair of adjacent two-dimensional electron gases (2DEGs), which were confined in coupled and uncoupled $Al_xGa_{1-x}As/AlAs/Al_yGa_{1-y}As$ double quantum wells (DQWs), as a function of front-gate voltage (V_g). The electron densities and mobilities of the first and second sub-bands were determined using the fast Fourier transform (FFT) in both coupled and uncoupled samples, named S1, S2 and S3, which have different aluminum (Al) content in each well. Sample S1 was illuminated in order to reach the coupled behavior. The electronic properties of the samples have been compared, showing that the electron density and mobility decrease with increasing Al content within the quantum wells (QWs). The last fact was attributed to the alloy scattering in the $Al_xGa_{1-x}As$ quantum well.

1. Introduction

In the last decades there have been a lot of experimental as well as theoretical studies on the electronic transport properties of two dimensional electron gas (2DEG) confined in $Al_xGa_{1-x}As/GaAs/Al_xGa_{1-x}As$ double quantum wells (DQWs), coupled by tunneling [1–5]. When the quantum wells in the DQW are adjusted to be symmetric such that the energy levels in their bands coincide, the wave functions are strongly mixed to form symmetric and anti-symmetric states, separated by the energy gap Δ_{SAS}, which depends on the barrier width between the wells. In this case the electrons have equal probabilities of being found in either of the two wells. As the system moves away from the symmetry, the two bands become progressively localized in either well, which is known as the uncoupled case. On the other hand, it is well known that the $Al_xGa_{1-x}As$ is a potentially important semiconductor material for many optical and microwave devices because of the continuous variability of the band gap and band structure, which varies with alloy composition and offers a good control over the energy levels and electrical properties [6–10], being the modulations of the Landé g factor one of the most important applications [11–13].

* Corresponding author. Tel./fax: +55 55 3421 8400.
** Corresponding author.
E-mail addresses: legarmas@gmail.com (L.E.G. Armas), celso@fisica.ufpr.br (C.A. Duarte).

http://dx.doi.org/10.1016/j.physe.2014.04.001
1386-9477/

Transport properties on $Al_xGa_{1-x}As$ alloys have shown that electron mobility and Hall density decrease with increasing Al concentration. In unintentionally doped alloys the mobility is weakly dependent on Al concentration in the composition range $0<x<0.3$, where typical values of the mobility are in the range from 3×10^3 cm^2/V s to 5×10^3 cm^2/V s [14]. On the other hand for x values exceeding 0.3, the mobility decreases very abruptly with the Al composition until reaching a minimum at $x\sim0.45$ [14]. Alloy scattering in $Al_xGa_{1-x}As$/GaAs heterostructures was considered firstly by Ando [15] in $Al_xGa_{1-x}As$ barriers, and later in InP/$In_xGa_{1-x}As$ quantum wells [16–18]. This effect was considered in our measurements due to the different Al concentration in each quantum well.

In this work we have studied three samples, with a structure of coupled and uncoupled DQWs with different Al content within the QWs, and it is organized in two parts, in the first part we provide information about the structure of the samples and details of the experimental setup. In the second part, the electron concentration and mobility of each occupied sub-band determined from Shubnikov-de Haas (SdH) and Hall measurements are shown for the coupled and uncoupled samples. The uncoupled sample was analyzed before and after being illuminated, showing in both cases that the QW with lower Al content has better electronic properties than the QW with higher Al concentration. In general, it was demonstrated that the electronic properties of the $Al_xGa_{1-x}As$ QWs decrease as the Al concentrations increase within the wells. The final section presents the conclusions of the work.

2. Samples and experimental details

The three samples under investigation consisted of remotely δ-doped $Al_xGa_{1-x}As$ double quantum wells grown by solid source molecular beam epitaxy on undoped (1 0 0) GaAs substrates. The spacers between the wells and the doped layer consisted of an AlAs/GaAs short-period superlattice with 12 periods of 4 monolayers of AlAs and 8 monolayers of GaAs. Two remote Si δ-doping sheets (concentration 2.2×10^{12} cm^{-2}) provided n character to the samples. The samples were named S1–S3, and each quantum well of the DQW sets on these samples had the same width $d_W=140$ Å although not necessarily the same Al content. In sample S1, the well nearest to the substrate (lower quantum well, QW_1) had $x=8.9\%$ Al content and the nearest to the surface (upper quantum well, QW_2) had $x=14.0\%$ Al content. In this sample the wells were separated by a $d_b=50$ Å width AlAs central barrier. Because of the different Al content in the wells, sample S1 had a weak asymmetry that was compensated by the introduction of an additional thinner spacer layer between the doped layer and the QW_1. On the other hand, the sample S2 has the same structure as sample S1 with a AlAs barrier thickness of approximately four times thinner than S1 ($d_b=14$ Å) and equal Al concentration on both wells ($x=10\%$). Finally, the quantum wells of the sample S3 were growth only with GaAs ($x=0.0\%$) in each one, being separated by a $d_b=14$ Å width AlAs barrier.

By a standard lithographic process it was constructed a Hall bar structure on the samples, to which it were soldered ohmic contacts to the two-dimensional channel by the diffusion of metallic In. The active region of the Hall bars was covered by a Ti/Au front gate electrode (Schottky contact) which enabled to tune the sub-band occupation in a controlled way by the application of a gate voltage V_g, between this front gate and the two-dimensional channel.

SdH and Hall measurements were performed at low temperature in a liquid He bath cryostat inserted into a superconducting coil using standard lock-in technique. Measurements were made for different gate voltages and on the range of applied magnetic field B from zero up to 11.0 T, perpendicular to the 2DEG, for all the studied samples. The applied current was typically about 1 μA, and the measurements were performed at $T=1.6$ K. The SdH measurements were used to obtain the density and quantum mobility of the electrons in each sub-band. The experimental data were numerically differentiated, expressed as a function of the reciprocal field ($1/B$) and analyzed using a fast Fourier transform (FFT) algorithm. In order to determine the concentration of each sub-band with more accuracy, the magnetoresistance traces were multiplied by the Hanning-window function before computing their FFT to produce better-resolved Fourier spectra [19]. The electron sub-band densities were related to the frequencies f_i of the SdH oscillations by the expression $n_i=2ef_i/h$ where e is the electron charge and h is Planck's constant. The total free-electron density n_T was determined by summing the individual electron densities of all the occupied sub-bands, $n_T=\sum_i n_i$. The quantum mobility of each sub-band was determined from the SdH measurements by the logarithmic dependence of the maximum amplitude of the FFT peak plotted against $1/B$. In these conditions, the slope of the straight line through the data is equal to π/μ_i [20].

3. Results and discussions

3.1. Electronic structure determined by self-consistent calculations

In order to provide theoretical information about the electronic structure of the DQW structures (band bending, sub-band energies and occupancy, and envelope wave functions), self-consistent calculations were performed. Quantized energy levels were calculated by simultaneously solving Schrodinger and Poisson equations within the context of the effective-mass formalism. The exchange and correlation effects were considered in the local density approximation [21–23]. The input parameters to the calculations comprised GaAs and $Al_xGa_{1-x}As$ parameters (effective masses, dielectric constants, and band offsets), the width of the wells and barriers.

The results of calculations are shown in Figs. 1–3. In these figures are shown, (a) the profiles of the conduction band on the active regions, (b) the electron density profiles, and (c) the electron sheet densities (total n_s and density of each sub-band, $n_{1,2}$) as a function of the applied electric field. The total electron sheet density n_s at zero gate voltage was used as input in the calculations and chosen to obtain the best agreement with the results of FFT data presented in Section 3.2 (i.e. the best accordance between Figs. 1c, 2c, 3c and 5b, 7b, 8b, respectively). For sample S1, the best fit was achieved considering the existence of a built-in electric field of 3.4×10^6 V/m, which is justified by the asymmetry associated to its differentiated architecture on one of the spacer layers.

For this sample, at $V_g=0$ the electron density is mainly concentrated on the left well (with the lower Al content), as expected (see Fig. 1b). On the other side, samples S2 and S3 are in balance states at $V_g=0$ (equal electron densities in both wells), since both have the same Al content (see Figs. 2 and 3).

The main results of Figs. 1–3 are Figs. 1c, 2c and 3c, which will be analyzed in sequence. In Fig. 1c, we verify that the increase of the electric field in sample S1 results on the simultaneous increase of n_s and n_1 while, contrary to the expected, the population on the second sub-band remains almost unchanged, with a soft downward trend. This effect is explained by the small lowering of the bottom of the QW_2 with the reduction of the electric field (Fig. 1a), resulting on a gradual increase on the population of QW_2 that impacts directly on n_2 (it was verified that the sub-band sheet densities $n_{1(2)}$ coincide with the electron population of $QW_{2(1)}$ up to a precision typically lower than 1%). On the other side, the

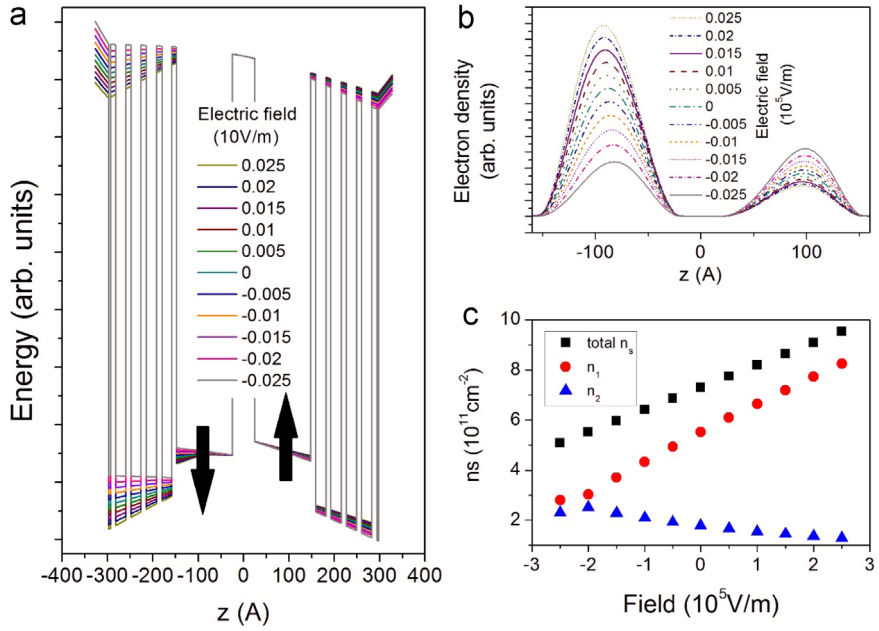

Fig. 1. Results of self-consistent calculations for sample S1: (a) the profile of the conduction band, (b) the total electron density, and (c) the electron sheet densities (total sheet density n_s, and the sheet densities of each sub-band, $n_{1,2}$). In (a), the arrows point the deflection of the conduction band with the increase of the field. It was verified that the sub-band sheet densities $n_{1,2}$ coincide with the electron population on each quantum well up to a precision typically lower than 1%.

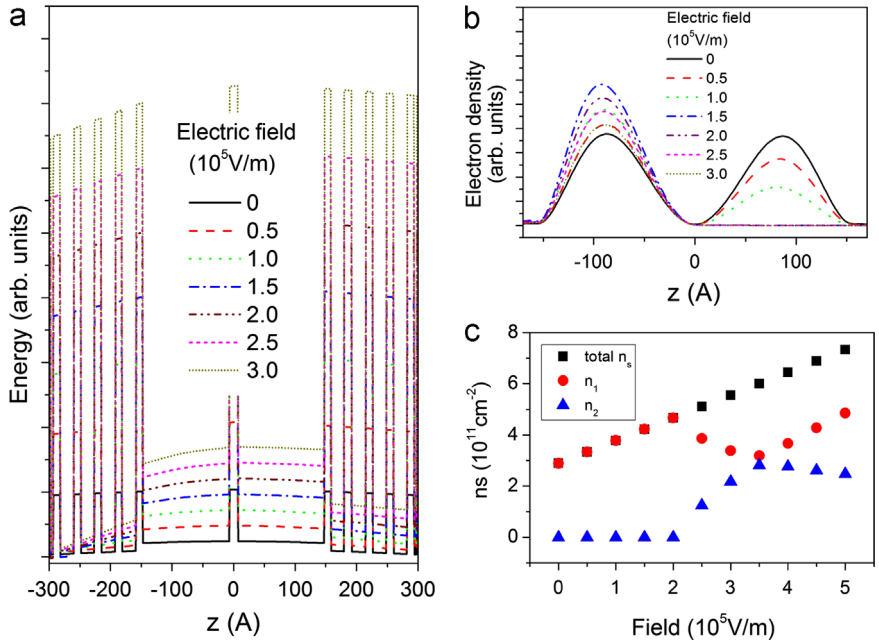

Fig. 2. Results of self-consistent calculations for sample S2: (a) the profile of the conduction band, (b) the total electron density and (c) the electron sheet densities (total sheet density n_s, and the sheet densities of each sub-band, $n_{1,2}$). It was verified that the sub-band sheet densities $n_{1,2}$ coincide with the electron population on each quantum well up to a precision typically lower than 1%.

deflection of the bottom of the QW_1 is pronounced, and since in most cases the bottom of QW_1 is below the bottom of the left one, the population of this well is usually higher.

For the case of Figs. 2 and 3c, the behavior is essentially different from that in Fig. 1c. While the electron density increases with the increase of the electric field, the second sub-band remains completely depleted for fields below 2×10^5 V/m. The onset of population of this sub-band is accompanied by a small depletion of the first sub-band, until the condition of equal population of both sub-bands is achieved (at 3.5×10^5 V/m in Fig. 2c, and at 5×10^5 V/m in Fig. 3c). Further increase of the electric field leaves to a gradual depletion of the second sub-band in samples S2 (Fig. 2c) and S3 (yet not visible in the range of fields in Fig. 3c).

Table 1 shows a comparison between results obtained by the self-consistent calculations (theory) and experimental data (presented in Section 3) for samples S1–S3 at $V_g=0$. In this table, one observes good agreement between theoretical and experimental results obtained for the three samples. Particularly, the large difference between the values of the first and second sub-bands means that the sample S1 is in an unbalance state. The balance and unbalance states at $V_g=0$ are confirmed by the evaluation of the electron density within each well, which are shown in the two last columns of Table 1. On the other hand, Table 2 shows

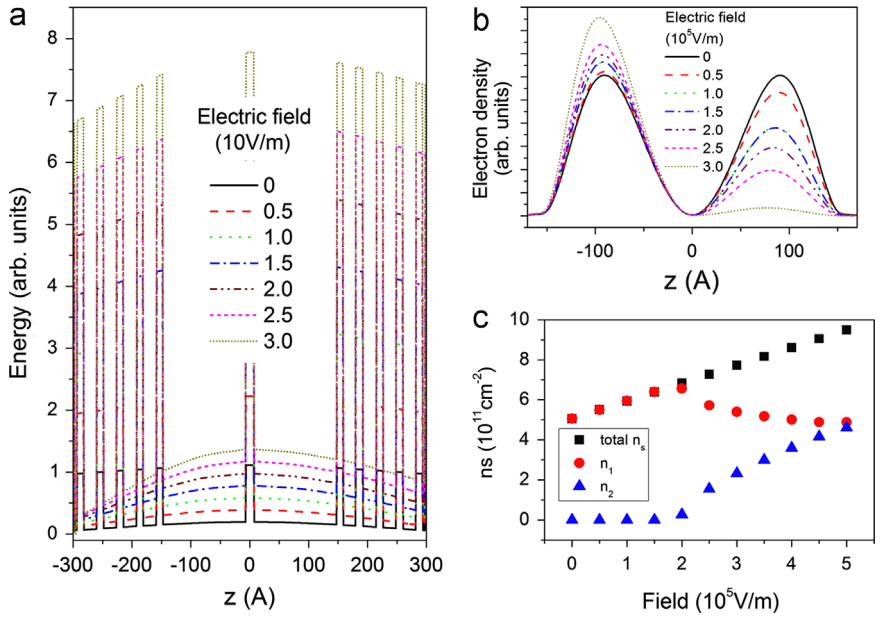

Fig. 3. Results of self-consistent calculations for sample S3: (a) the profile of the conduction band, (b) the total electron density and, (c) the electron sheet densities (total sheet density n_s, and the sheet densities of each sub-band, $n_{1,2}$). It was verified that the sub-band sheet densities $n_{1,2}$ coincide with the electron population on each quantum well up to a precision typically lower than 1%.

Table 1
Comparison between theoretical and experimental sub-band electron densities (n_i) and the densities of the individual wells (n_{QW}) obtained from the numerical integration of the charge-density profile of each well. The densities are in units of 10^{11} cm^{-2}.

Sample	d_b (Å)	n_i (theory)		n_i (experiment)		n_{QW}	
		n_1	n_2	n_1	n_2	n_{QW1}	n_{QW2}
S1	50	6.78	1.85	6.06	1.79	6.7	1.8
S2	14	3.84	3.28	3.71	3.06	3.6	3.6
S3	14	5.12	4.26	4.93	4.05	4.5	4.5

Table 2
Theoretical and experimental energy gaps for samples S1–S3.

Sample	Δ_{12} (meV)	
	Theory	Exp.
S1	16.2	14.1
S2	1.85	2.1
S3	2.84	2.9

a comparison between the theoretical and experimental energy differences Δ_{12} between the first and second sub-bands for all samples, showing good agreement.

3.2. Experimental data

3.2.1. Sample S1

Due to the unbalance state on the electron density of each well, this sample was illuminated. Therefore results before and after illumination will be presented.

3.2.1.1. Before illumination. Fig. 4 shows the result of SdH measurements at 1.6 K for two different values of V_g, 0.0 V and −0.4 V. Fig. 4a presents the result for V_g=0.0 V, where it can be seen a complex pattern of SdH oscillations due to the superposition of two SdH frequencies from the two occupied sub-bands (denoted by the

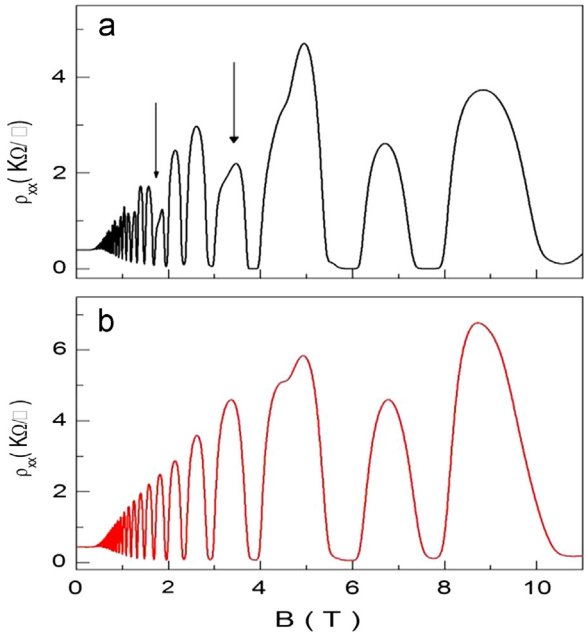

Fig. 4. SdH curves of sample S1 recorded at T=1.6 K for two different values of front gate voltages. (a) V_g=0.0 V and (b) V_g=−0.4 V. The arrows in (a) denote the beating of the two different SdH frequencies of the two sub-bands.

black arrows). In Fig. 4b, we observe a single SdH oscillation at low magnetic field, for V_g=−0.4 V, indicating that only one sub-band is populated.

Fig. 5a shows FFT spectra of the SdH oscillations of sample S1 for different gate voltages. The magnetic field interval to construct the FFT spectra was from 0.2 T to 1.5 T, which avoids the region where the integer quantum Hall effect (IQHE) occurs (at high field). Two occupied sub-bands (n_1 and n_2) were discernible for $V_g > -0.1$ V while for $V_g \leq -0.3$ V only one (n_1) sub-band was detected. In other words, the SdH oscillations exhibit only one frequency for $V_g \leq -0.3$ V, indicating that only the QW_1 is populated similarly as in Fig. 4b, where it is possible to see only one SdH oscillation (peak $n'_1 = 2n_1$ is an harmonic of peak n_1). The electron

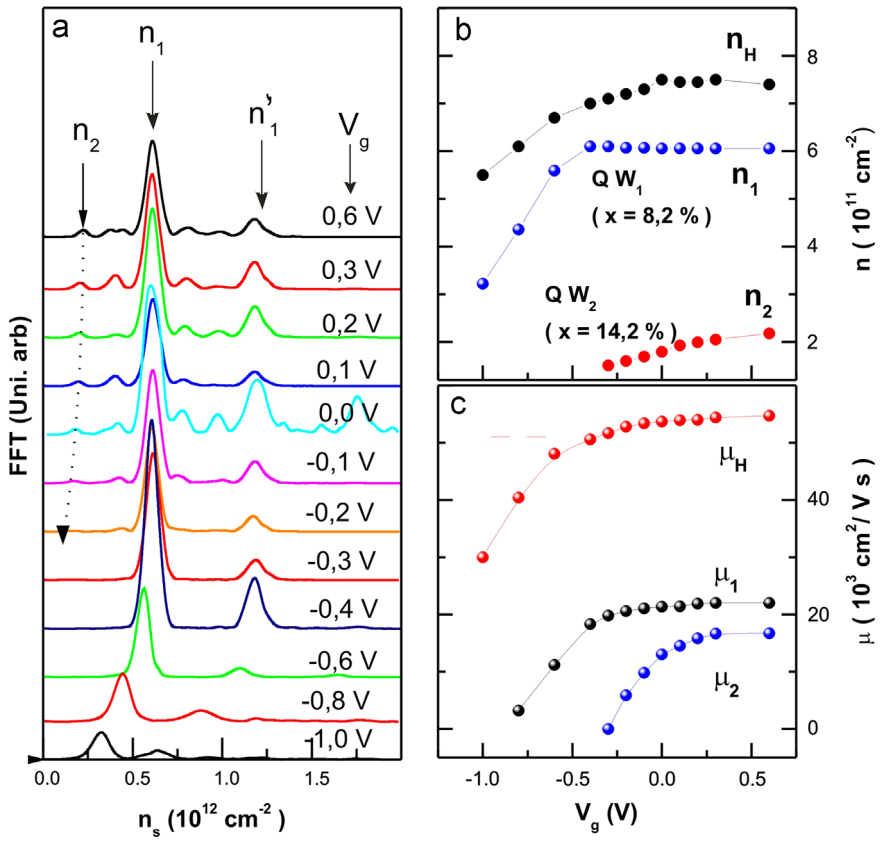

Fig. 5. (a) FFT spectra of the SdH oscillations of sample S1, varying the front gate voltage from $V_g = -1.0$ V (bottom) to $V_g = 0.6$ V (top). (b) Electron density of each occupied sub-band and total carrier concentration $n_T = n_1 + n_2$ obtained from the FFT spectra of (a). (c) Quantum mobilities of the two sub-bands as a function of the applied gate voltage determined from SdH data and low-field Hall mobility. The lines connecting the symbols are guides to the eyes.

densities of each sub-band (extracted from the FFT spectra of Fig. 5a) together with Hall densities are presented in Fig. 5b. In this figure we can see that there is a large difference between the electronic sub-bands n_1 and n_2. It is well known that the SdH oscillations measure the electron densities of the sub-bands, which not always agree with the electron densities of the individual layers [24] (in our case, the individual wells). However, for the data shown in Fig. 5b where the difference between n_1 and n_2 is well resolved, the sub-band wave functions are well localized in each QW, so that we can regard the first sub-band (n_1) and second sub-band (n_2) as the electron densities in QW_1 and QW_2. These experimental results are in accordance with the results obtained by the self-consistent calculations, where it was verified that the sub-band sheet densities $n_{1,2}$ coincide with the electron population on each quantum well $n_{QW1,2}$ up to a precision typically lower than 1% for all the ranges of applied electric field shown in Figs. 1–3.

Yet in Fig. 5b, we see that the electron density of the most populated sub-band (n_1), localized in the lower well ($x = 8.9\%$), remains almost constant in the range $-0.3 \le V_g \le 0.6$ V, whereas the peak of the second sub-band continuously decreases up to -0.2 V when it disappears. The constancy of n_1 is accompanied by the constancy of the total electron sheet density n_s, revealing that a mechanism prevents any variation of the population of the active region with the change of applied field. Such apparent constancy of the carrier density with the application of an external field was previously verified also in gated triple quantum wells [26], to which we attribute a not yet known phenomenon of charge transfer and accumulation on the complex structure of the samples. We stress that besides the wells and the superlattice barriers (whose structures were described above), the samples contain superlattice cap layers and about 50 nm of GaAs cap, with a surface delta doping to compensate the charges of free dangling bonds at the surface. We may consider that eventually the apparent depopulation of the second sub-band is within a margin of error, owing to the poor resolution of the peak n_2 on the FFT spectra of Fig. 5a.

In fact, if we compare Fig. 5b with Fig. 1c, we arrive to the conclusion that n_2 remains almost constant and on the order of 2×10^{11} cm^{-2}, and believe that only if FFT spectra were obtained with a better resolution we could find a similar behavior. In fact, by reasons explained in Section 3.1, we expect that the peaks n_1 and n_2 would be close together at larger negative fields. These arguments leave to a consistence between the FFT results and the self-consistent calculations.

In order to quantify the changes observed in the relative amplitude of the Fourier peaks presented in Fig. 5a, the quantum mobility of each sub-band was determined using the procedure mentioned in Section 2. Results of quantum mobility of each sub-band are shown in Fig. 5c, where it is also possible to see the Hall mobility as a function of V_g. As a matter of fact, the electron quantum mobility of the fundamental state μ_1 is higher than the quantum mobility of the excited state μ_2, and this occurs in all the range of the applied gate voltage, where both sub-bands were observed. In order to explain these facts, it will be analyzed two situations:

First – Several groups have determined in conventional modulation doped single QWs, at the absence of any applied gate voltage, that the electron quantum mobility is higher in the fundamental state (first sub-band) than in the first excited state (second sub-band) [14,16,17]. They explain their results in terms of (a) the physical separation of the electron distribution from the ionized donors, which reduces scattering as its separation from the ionized impurities in the δ-doped layer increases; (b) the Fermi

velocity of the carriers, which is lower in the higher sub-bands, resulting in increasing scattering and, therefore, lower mobility for decreasing applied gate voltage. In our case, we believe that the lower mobility of the second sub-band is a consequence of the smaller Fermi-wave vector k_{F2} compared to k_{F1} of the first sub-band. Observing Fig. 5b and c, we note a close relation between the behavior of the mobility and the electronic occupancy of the sub-bands. For instance, μ_1 starts to decrease when n_1 begins to be depleted (for $V_g < -0.2$ V). Using the Hall density (n_{Hall}) and mobility (μ_{Hall}) and the concentration of the sub-bands (n_1 and n_2) measured by SdH, we determined the transport mobilities μ_{1t} and μ_{2t} of the two occupied sub-bands, solving the equations system of the two-band conduction model [1,25]

$$\mu_{Hall} = \frac{n_1\mu_{1t}^2 + n_2\mu_{2t}^2}{n_1\mu_{1t} + n_2\mu_{2t}}, \quad n_{Hall} = \frac{n_1\mu_{1t} + n_2\mu_{2t}}{\mu_{Hall}}.$$

It was verified that the ratio μ_{it}/μ_{iq} ($i=1, 2$) is close to 2.5 in the range 0.0 V $\le V_g \le$ 0.6 V for both populated sub-bands, but showed a small change in the range $-0.3 \le V_g \le -0.1$ V. We obtained μ_{it}/μ_{iq}=2.7, 2.8, and 3.0 for $V_g = -0.1$, -0.2, and -0.3 V, respectively. Das Sarma and Stern [18] showed theoretically $\mu_{it}/\mu_{iq} = 2.5$ for ionized impurity scattering in a GaAs/AlGaAs heterostructure without a spacer containing a single sub-band with an electron density of 3.5×10^{12} cm^{-2}, in agreement with the value obtained for the structure here analyzed. Although the system here analyzed is a different type of heterostructure, the ratio of the transport and quantum mobilities suggests us that impurity scattering could be the main scattering mechanism actuating on the carriers. Before considering this hypothesis as true, it is worth to say that the Si dopants are separated from the QWs by a large GaAs/AlAs short period superlattice, reducing the ionized impurity scattering associated to the doping [27].

Second – Another way to explain why the quantum mobility of the first sub-band is higher than the second one is to suppose that this is due to the alloy disorder scattering present in the $Al_xGa_{1-x}As$ individual quantum wells. Taking into account this statement as true, we must prove that the electronic properties (electron densities and mobilities) in sample S1 and the other studied samples depend on the Al concentrations. For this purpose the wells of the sample S1 will be analyzed in an independent way, and it will be proved that the peak n_2 (shown in Fig. 5a), corresponding to the second sub-band is not spurious. For this purpose, sample S1 was illuminated in order to have a better resolution of the peak corresponding to the second sub-band (shown in Fig. 5a).

3.2.1.2. After illumination. Fig. 6a shows FFT spectra of the SdH oscillations of the illuminated sample in a voltage range of -1.2 V $\le V_g \le$ 0.7 V. The comparison of this figure with Fig. 5a reveals that after illumination the peak n_2 corresponding to the second sub-band increased, showing that the quantum lifetime τ_q and the quantum mobility of the second sub-band increased (since as it is well known, they increase with the height of the FFT amplitude [28]). The monotonic behavior of this peak with decreasing gate voltage assures that this peak corresponds to the second sub-band and not to a spurious peak. Similarly to the case of sample S1 prior to illumination, the amplitude of the peak n_1 corresponding to the first sub-band remains constant in almost all the range of applied gate voltages.

Fig. 6b shows the electron density of each sub-band extracted from FFT spectra of Fig. 6a, where it is possible to see that after the illumination of the sample the electron densities remain almost constant (compare with Fig. 5b), while the Hall density increases (at V_g=0.0 V it changed from 7.4×10^{11} cm^{-2} to 10.4×10^{11} cm^{-2}). Fig. 6c shows that the quantum motilities of the first/second sub-bands or electrons localized in the QW_1 (8.9%)/QW_2 (x=14.0%) remain almost constant in the overall range of the applied gate voltage and it is in agreement with the height of the FFT amplitude. The main characteristic in this figure is the increase in the Hall mobility about three times if compared to Fig. 5c. In the voltage range of -0.3 V $\le V_g \le$ 0.7 V the ratio μ_{it}/μ_{iq} increases from 2.5 to 12.7 in both populated sub-bands. The increases on the Hall density and mobility are expected since the illumination removes electrons from deep traps to the 2DEG, which are not efficiently recaptured by the deep states (once the light is turn off) due to potential barriers surrounding the active region [29,30].

3.2.2. Sample S2

Here it will be presented results related to a sample with equal Al contents inside the wells (x=10%), which results in a completely symmetric DQW. For this sample, the values of the electron densities are very close for gate voltages $V_g > -0.25$ V, as confirmed by the proximity of the peaks corresponding to the first and second sub-bands (see Fig. 7a) and also by the self-consistent calculations (compare with Fig. 2c). At V_g=0.0 V self-consistent calculations gives Δ_{12} =1.85 meV while the SdH oscillations gives Δ_{12}=2.1 meV. Due to the proximity of the first and second sub-bands (low value of Δ_{12}), it is not possible to resolve the two peaks n_1 and n_2 on the FFT spectra in Fig. 7a. However, we follow the behavior of their harmonic peaks $n'_1 = 2n_1$ and $n'_2 = 2n_2$, with which we estimate the occupancy of the sub-bands, as presented on Fig. 7b. As in sample S1, the occupation of the second sub-band (n_2) continuously decreases with the decrease of the gate voltage, and vanishes for $V_g < -0.6$ V. Note the increase of the energy separation between the two sub-bands, as V_g becomes more negative, which is the reason why the peaks n_1 and n_2 can be resolved for $V_g = -0.4$ and -0.6 V (see Fig. 7a). We have found $\Delta_{12} \approx 1.7$ meV for positive values of the gate voltages, which increases up to 6 meV for $V_g = -0.6$ V. Moreover, with decreasing negative bias, the energy of the well closest to the sample surface is raised, and electrons from this well are transferred to the other one, as observed by the small increase of n_1 for $V_g \le -0.4$ V. In order to verify if the electron densities obtained from the harmonic peaks are correct, we have made a sinusoidal fit of a measurement of the magnetoresistance with the Lifshits–Kosevich equation with two populated sub-bands at zero gate voltage and in low magnetic field (from 0.0 T to 0.6 T) (not shown here), from which we obtained $n_1 = 3.81 \times 10^{11}$ cm^{-2} and $n_2 = 3.42 \times 10^{11}$ cm^{-2}, that are also in good agreement with the values in Table 1 for sample S2 ($n_1 = 3.84 \times 10^{11}$ cm^{-2} and $n_2 = 3.28 \times 10^{11}$ cm^{-2}). On the other hand, the values obtained from the harmonic peaks were $n_1 = 3.71 \times 10^{11}$ cm^{-2} and $n_2 = 3.06 \times 10^{11}$ cm^{-2} at zero gate voltage, that are also in good agreement with the theoretical results and the data obtained from n'_1 and n'_2. Note also that quantum lifetimes obtained from the exponential terms of the Lifshits–Kosevich were almost equal for the two sub-bands ($\tau_{q1} \approx \tau_{q2} = 1.2$ ps), and consequently so do their quantum motilities. Fig. 7c shows the Hall mobility of this sample as a function of V_g. Due to the close proximity of the peaks n_1 and n_2 in Fig. 7a, it was not possible to calculate their respective quantum motilities.

3.2.3. Sample S3

For this sample with two pure GaAs QWs (x=0%), the magnetotransport measurements were performed on a range of magnetic field from 0 T to 1.5 T (to avoid spin and quantum Hall effects) for gate voltages from 1.0 V to -1.5 V in steps of 0.1 V. The resulting FFT spectra are shown in Fig. 8a. We clearly see two well resolved peaks n_1 and n_2, which correspond to the first and the second sub-bands, respectively, and the harmonic n'_2 of the second sub-band. Fig. 8b shows the extracted electron densities, where n_1 is related

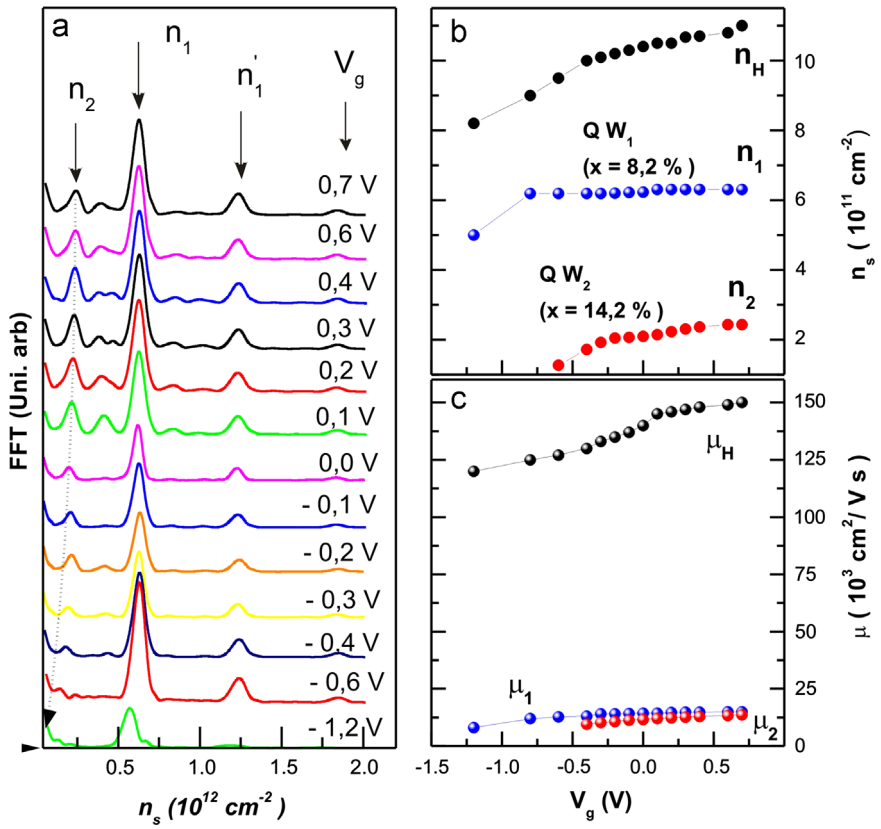

Fig. 6. Data for sample S1 after illumination: (a) FFT spectra of the SdH oscillations from $V_g = -1.2$ V (bottom) to $V_g = 0.7$ V (top); (b) electron density of each occupied sub-band and total carrier concentration $n_T = n_1 + n_2$ obtained from the FFT spectra; (c) quantum mobilities of the two sub-bands, determined from SdH data and low-field Hall mobility as a function of V_g.

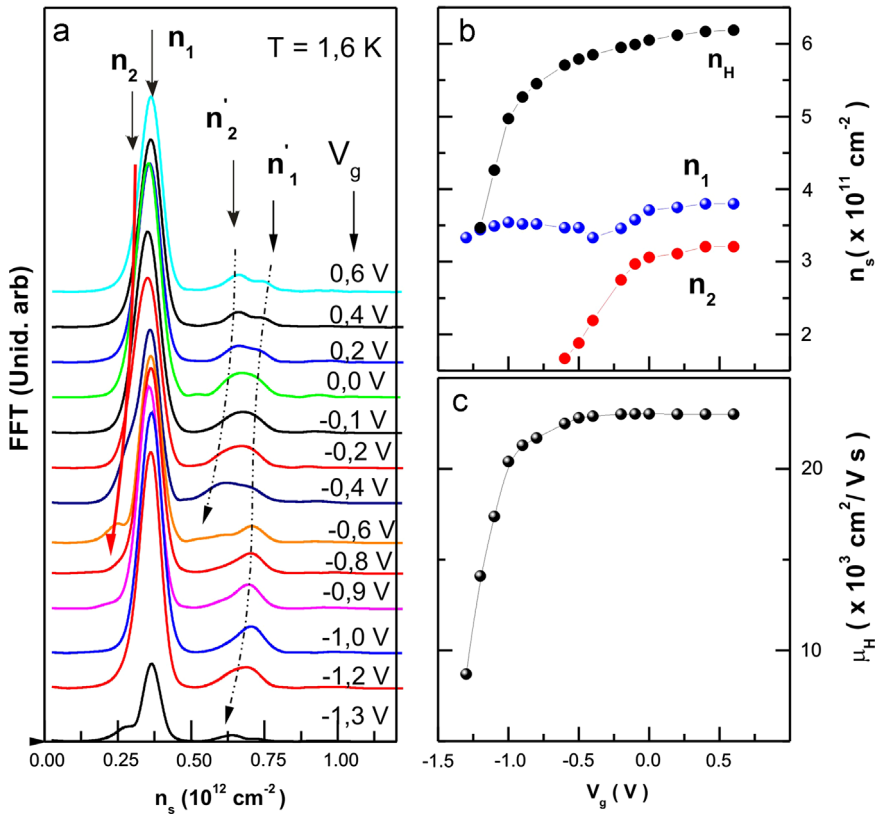

Fig. 7. (a) FFT spectra of the SdH oscillations at the range of voltages $-1.3\ \text{V} \le V_g \le 0.6$ V, for sample S2; (b) electron density of each occupied sub-band obtained from the FFT spectra and the Hall concentration (n_{Hall}); (c) low field Hall mobility.

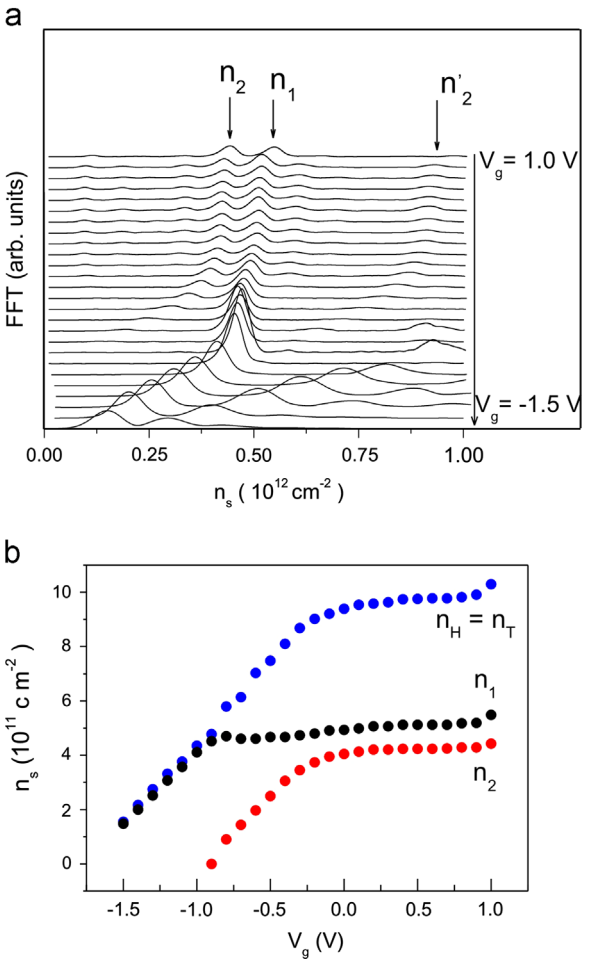

Fig. 8. (a) FFT spectra of the SdH oscillations of sample S3 at the range of voltages $-1.5\ \mathrm{V} < V_g < 1.0\ \mathrm{V}$; (b) electron densities of each occupied sub-band obtained from the FFT spectra and the Hall density (n_H) which coincide with the total electron density (n_T).

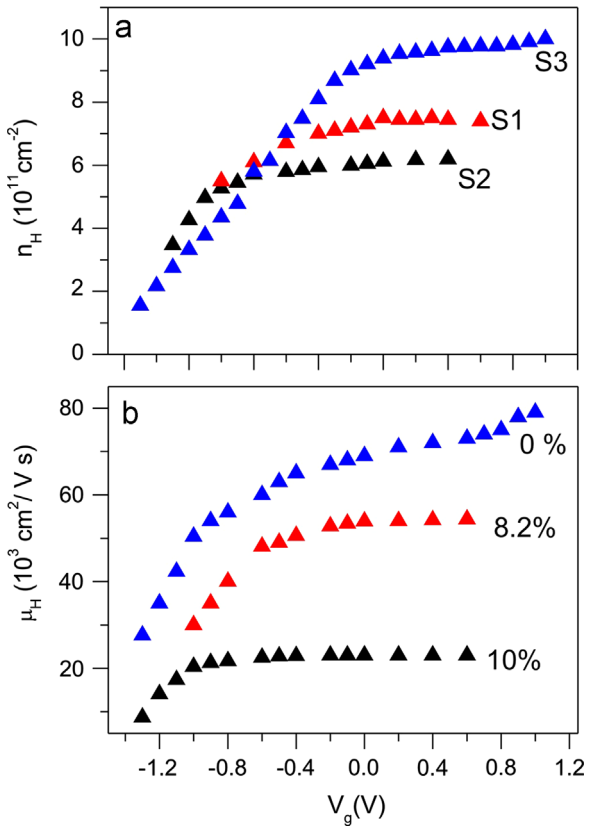

Fig. 9. Comparison of the Hall densities (a) and mobilities (b) of the three samples as a function of V_g. The Hall density and mobility are lower in the sample with higher Al content within the QWs.

with electrons in QW_1 and n_2 to electrons in QW_2, similarly to the case of samples S1 and S2, as a function of the gate voltage decrease. The electron density of the first sub-band remains almost constant for $-0.8\ \mathrm{V} < V_g < 1.0\ \mathrm{V}$ and the Hall density coincides with the total electron density. Also, the heights of the FFT amplitudes of n_1 and n_2 are almost equal for $V_g > 0.9\ \mathrm{V}$, which means that the quantum motilities of both sub-bands are close.

With the results of the electronic properties of the three samples, now we will perform a comparison among them. Fig. 9a and b shows that the Hall concentration and mobility of the three samples have similar behavior in all the range of the applied gate voltage. We observe that the Hall density of sample S3 is higher than that of the samples S1 and S2. It is worth to emphasize that the Al contents within both wells of the sample S3 is $x=0\%$ (QWs of GaAs) and $x=10\%$ for the sample S2, while for sample S1, the QWs have different Al contents, $x=8.9\%$ (QW_1) and $x=14.0\%$ (QW_2). We can note that the QWs of sample S1 have, in average, higher Al content than the wells of the sample S2 and, therefore, the Hall density and mobility for the sample S2 should be higher than the Hall density and mobility for the sample S1. This means that the major contribution to the electronic properties, of sample S1, stems from the QW with lower Al concentration. This statement is proved by results shown in Figs. 5b and 6b. Fig. 5b shows that the majority of electrons are localized in the QW_1 in the whole interval of the gate voltage, which is confirmed by the self-consistent calculations for $V_g=0.0\ \mathrm{V}$. It is worth to note that for $V_g=0.0\ \mathrm{V}$ (Fig. 5b) the electron density of the first sub-band, $n_1=6.1\times10^{11}\ \mathrm{cm}^{-2}$, is comparable to the value of the Hall density ($7.5\times10^{11}\ \mathrm{cm}^{-2}$). Taking into account the value of the ratio, $\mu_{1t}/\mu_{1q}=2.5$, at zero gate voltage, it is possible to calculate the transport mobility of the first sub-band, $\mu_{1t}=2.5\mu_{1q}=53.0\times10^3\ \mathrm{cm}^2/\mathrm{V\,s}$, almost equal to the Hall density ($\mu_H=53.7\times10^3\ \mathrm{cm}^2/\mathrm{V\,s}$). Therefore, from these results, we can argue that the main contribution to the Hall density and mobility, for the sample S1, is due to the electrons localized in the QW_1 where the Al concentration is $x=8.9\%$. This is the reason why the electron density and Hall mobility are higher for sample S1 than for the sample S2 (where $x=10\%$). A similar situation was reported in AlAs/$Al_{0.1}Ga_{0.9}As$ bilayers [31], where by modulating the front and back gate voltages was possible to have SdH oscillations in any of the bilayers in an independent way. Fig. 9b also shows that the sample with lower Al concentrations has higher Hall mobility.

Finally, it is well known that the band structure of $Al_xGa_{1-x}As$ can be described with a three-band model Γ, X and L of the Brillouin zone, for all values of x ($0<x<1$). This model allows us to analyze the electronic properties in $Al_xGa_{1-x}As$ alloys as established by Saxena [6,7,32]. For $0\le x\le0.32$, the minimum at Γ is the lowest-energy minimum and the effect of electrons in the L and X minima on the Hall mobility can be neglected to a good approximation, while for $0.6\le x\le1.0$, the minimum at X is the lowest energy and the contributions from Γ and L minima can be ignored. On the other hand, for intermediate compositions, $0.32\le x\le0.6$, the contributions from all three minima must be considered, since they lie close to each other in energy [33]. Since in our samples $0\le x\le0.32$, the Γ point has the lowest-energy and is the relevant in the transport properties. It is known that the

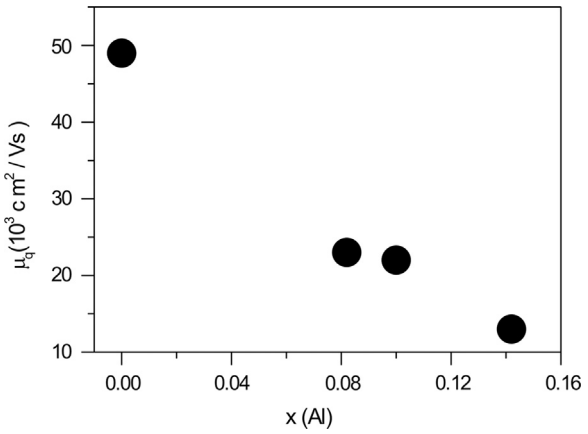

Fig. 10. Quantum mobility of the first sub-band for samples S1–S3 as a function of the Al concentrations, for V_g=0.0 V.

electron mobility μ_Γ in the Γ minimum of GaAs varies inversely with $m_\Gamma^{*3/2}$ [33,34], where m_Γ^* is the electron effective mass in the Γ conduction-band minimum. Since the increase of x implies on the increase of m_Γ^*, the mobilities μ_Γ and μ_H are reduced [33]. Such decrease on μ_H has been found on ternary alloys of the systems $GaAs_{1-x}P_x$ [35] and $Ga_{1-x}In_sAs$ [36].

Fig. 10 shows the quantum mobility of the first sub-band, for V_g=0 V for all the studied samples as a function of the Al concentration. It is observed that the quantum mobility within the wells decreases with x. Therefore, we can argue that the worsening of the electronic properties with the increase of the Al concentration is due to the alloy scattering present in the $Al_xGa_{1-x}As$ QWs and not to the impurity-scattering mechanism as it was supposed before. It is worth to emphasize that the behavior of the electronic properties as a function of the Al content was very important to have a better understanding of the theoretical and experimental n_s–B phase diagrams of the samples S2 and S3 [37].

4. Conclusion

We studied the effect of Al concentration on the electronic properties of coupled and uncoupled $Al_xGa_{1-x}As/AlAs/Al_yGa_{1-y}As$ double quantum wells (QWs) of three samples. Experimental results of the uncoupled QWs (sample S1) before and after illumination, showed that the electron wave-functions of the occupied sub-bands are localized within each well in an independently way and that the QW with lower Al content has better electronic properties. These results are in a good agreement with those obtained by self-consistent calculations, for V_g=0.0 V, before illumination of the sample. On the other hand, experimental results for samples with equal concentration of Al within the wells showed that the quantum mobilities of the two occupied sub-bands are equal. In spite of the fact that the ratio between the transport and quantum mobilities is between 2 and 3 for both occupied sub-bands of the uncoupled sample, the ionized impurity scattering is not the limiting mechanism for the mobility due to the large spacer width (large period superlattice) between the ionized impurities and the 2DEG. A careful analysis leaves to the conclusion that the alloy scattering is responsible for the decrease of the electronic properties with the increase of the Al content within the $Al_xGa_{1-x}As$ QWs.

Acknowledgments

The authors would like to thank the Brazilian Agencies CNPq and CAPES for partial financial support. C. Jacinto thanks the program *PNPD/CAPES at the Universidade Federal de Alagoas* (*UFAL*) *through the Project no. 02727/09-9*.

References

[1] H.L. Stormer, A.C. Gossard, W. Wiegmann, Solid State Commun. 47 (1982) 707.
[2] R. Fletcher, M. Tsaousidou, T. Smith, P.T. Coleridge, Z.R. Wasilewski, Y. Feng, Phys. Rev. B 71 (2005) 155310.
[3] I. Lo, J.K. Tsai, P.C. Ho, W.J. Yao, C.H. Chang, J.C. Chiang, L.W. Tu, Phys. Rev. B 67 (2003) 195317.
[4] J.J. Harris, J.B. Van der Velde, C. Roberts, K. Woodbridge, K.M. Hutchings, Semicond. Sci. Technol. 6 (1991) 616.
[5] F. Bosc, J. Sicart, J.L. Robert, Semicond. Sci. Technol. 14 (1999) 64.
[6] A.K. Saxena, Phys. Status Solidi B 96 (1979) K77.
[7] A.K. Saxena, Appl. Phys. Lett. 36 (1979) 79.
[8] T. Ando, Rev. Mod. Phys. 54 (1982) 437.
[9] A. Palevski, F. Beltran, F. Capasso, L. Pfeiffer, K.W. West, Phys. Rev. Lett. 65 (1990) 1929.
[10] Y. Takagaki, K.J. Friedland, R. Hey, K.H. Ploog, Phys. Rev. B. 66 (2002) 035309.
[11] L.E.G. Armas, G.M. Gusev, A.K. Bakarov, N.F. Oliveira, J.C. Portal, Physica E 40 (2008) 156.
[12] V.H. Russel, S.N. Holmes, P. Atkinson, D.K. Maude, F. Sfigakis, D.A. Ritchie, M. Pepper, Semicond. Sci. Technol. 22 (2007) 722.
[13] G. Salis, Y. Kato, K. Ensslin, D.C. Driscoll, A.C. Gossard, A. Wshalom, Nature 414 (2001) 619.
[14] E. Skuras, R. Kumar, R.L Williams, R.A. Stradling, J.E. Dmochowski, E.A. Johnson, A. Mackinnon, J.J. Harris, R.B. Beall, C. Skierbeszewski, J. Singleton, P.J. Van der Wel, P. Wisniewski, Semicond. Sci. Technol. 6 (1991) 535.
[15] T. Ando, J. Phys. Soc. Jpn. 51 (1982) 3900.
[16] P.M. Koenraad, B.F.A. Van Hest, F.A.P. Blom, R. Van Dalen, M. Leys, J.A.A.J. Perenboom, J.H. Wolter, Physica B 177 (1992) 485.
[17] J.J. Harris, R. Murray, C.T. Foxon, Semicond. Sci. Technol. 8 (1993) 31.
[18] S. Das Sarma, F. Stern, Phys. Rev. B 32 (1985) 8442.
[19] A.B. Henriques, Phys. Rev. B 50 (1994) 8658.
[20] A. Cavalheiro, E.C.F. Da Silva, E.K. Takahashi, A.A. Quivy, J.R. Leite, E.A. Meneses, Phys. Rev. B 65 (2002) 075320.
[21] F. Stern, S. Das Sarma, Phys. Rev. B 30 (1984) 840.
[22] A.J. Rimberg, R.M. Westervelt, Phys. Rev. B 40 (1989) 3970.
[23] C.A. Duarte, Comput. Phys. Commun. 181 (2010) 1501.
[24] X. Ying, S.R. Parihar, H.C. Manoharan, M. Shayegan, Phys. Rev. B 52 (1995) R11611.
[25] S. Mori, T. Ando, Phys. Rev. B 19 (1979) 6433.
[26] C.A. Duarte, L.E.G. Armas, E.C.F. da Silva, G.M. Gusev, A.K. Bakarov, S. Wiedmann, J.C. Portal, Europhys. Lett. 94 (2011) 37010.
[27] K.J. Friedland, R. Hey, H. Kostial, R. Klann, K. Ploog, Phys. Rev. Lett. 77 (1996) 4616.
[28] I. Lo, W.C. Michael, M. Ahouja, J.P. Cheng, A. Fathimulla, H. Mier, App. Phys. Lett. 66 (1995) 754.
[29] I. Lo, D.P. Wang, K.Y. Hsieh, T.F. Wang, W.C. Mitchel, M. Ahoujja, J.P. Cheng, A. Fathimulla, H. Hie, Phys. Rev. B 52 (1995) 14671.
[30] A. Babinski, G. Li, C. Jagadish, Appl. Phys. Lett. 71 (1997) 1664.
[31] E.P. De Poortere, M. Shayegan, Appl. Phys. Lett. 84 (2004) 3837.
[32] A.K. Saxena, J. Phys. C Solid State Phys. 13 (1980) 4323.
[33] A.K. Saxena, Phys. Rev. B 24 (1981) 3295.
[34] A. Fortini, D. Diguet, J. Lugand, J. Appl. Phys. 41 (1979) 3121.
[35] M.G. Craford, W.O. Groves, Proc. IEEE 61 (1973) 862.
[36] R.W. Conrad, P.L. Hoyt, D.D. Martin, J. Electrochem. Soc. 114 (1967) 164.
[37] L.E.G. Armas, G.M. Gusev, T.E. Lamas, A.K. Bakarov, J.C. Portal, J. Mod. Phys. B 23 (2009) 2933.